

# Iterative summation of path integrals for nonequilibrium molecular quantum transport

R. Hütten,<sup>1</sup> S. Weiss,<sup>1,2</sup> M. Thorwart,<sup>2</sup> and R. Egger<sup>1</sup>

<sup>1</sup>*Institut für Theoretische Physik, Heinrich-Heine-Universität, D-40225 Düsseldorf, Germany*

<sup>2</sup>*I. Institut für Theoretische Physik, Universität Hamburg, D-20355 Hamburg, Germany*

(Dated: February 1, 2012)

We formulate and apply a nonperturbative numerical approach to the nonequilibrium current,  $I(V)$ , through a voltage-biased molecular conductor. We focus on a single electronic level coupled to an unequilibrated vibration mode (Anderson-Holstein model), which can be mapped to an effective three-state problem. Performing an iterative summation of real-time path integral (ISPI) expressions, we accurately reproduce known analytical results in three different limits. We then study the crossover regime between those limits and show that the Franck-Condon blockade persists in the quantum-coherent low-temperature limit, with a nonequilibrium smearing of step features in the  $IV$  curve.

PACS numbers: 73.63.-b, 72.10.-d, 02.70.-c

*Introduction.*—Understanding quantum transport in nanoscale electronic systems with vibrational or mechanical (“phonon”) degrees of freedom is of topical interest in several areas of physics, including molecular electronics [1, 2], inelastic tunneling spectroscopy [3], nanoelectromechanical systems [4], break junctions [5], and suspended semiconductor or carbon-based nanostructures [6–9]. The electron-phonon interaction allows to observe a rich variety of intriguing phenomena, such as negative differential conductance, the Franck-Condon blockade of transport, rectification, vibrational sidebands or steplike features in the current-voltage ( $IV$ ) characteristics, and current-induced heating or cooling. Already the simplest nonequilibrium “Anderson-Holstein” (AH) model, where the nanostructure corresponds to just one spinless electronic level coupled to a single oscillator mode, captures much of this richness [10, 11]; for a review, see Ref. [3]. Analytical approaches allow to understand the AH model in various corners of parameter space, but no controlled approximation, let alone exact solution, connecting these corners seems in reach. One may expect that a unified picture is available from numerics. However, numerical renormalization group [12] or quantum Monte Carlo (QMC) calculations [13, 14] are usually restricted to equilibrium. For the nonequilibrium AH model, Han [15] employed an imaginary-time QMC approach followed by a double analytical continuation scheme; unfortunately, the latter step is plagued by instabilities [16]. A promising avenue for the AH model has recently been suggested by real-time path-integral QMC simulations [17, 18], where one directly computes the time-dependent current. Such calculations have to deal with the infamous dynamical sign problem at long times, but in several parameter regions, especially when a secondary phonon bath is present, the stationary steady-state regime can be reached.

In this work, we formulate and apply an alternative numerical approach, which in practice is useful unless both the temperature  $T$  and the bias voltage  $V$  are small. It

is also based on a Keldysh path-integral formulation but does not involve stochastic sampling schemes and thus remains free from any sign problem. To that end, we extend the “iterative summation of path integrals” (ISPI) technique [19] to the AH model. Technical aspects of the present approach, in particular our mapping to an effective three-state system via the “spin-1 Hirsch-Fye transformation” in Eq. (2) below, should also be of interest to QMC schemes [14]. In essence, the ISPI method exploits that time correlations of the auxiliary three-state Keldysh variable, which arise after functional integration over the phonon and the (dot and lead) fermion degrees of freedom, can be truncated beyond a certain memory time  $\tau_m$  when either  $T$  or  $V$  is finite. Together with a convergence scheme designed to eliminate systematic errors due to the finiteness of  $\tau_m$ , such calculations allow to obtain numerically exact results. The ISPI method has already been successfully applied to the spinful Anderson model [19–21], where instead of the phonon a local charging interaction is present. While we focus on the simplest version of the AH model with a single unequilibrated [22] phonon mode here, the conceptual generalization to include Coulomb interactions, more phonon modes, or several dot levels is straightforward. We benchmark our ISPI code against three different analytical approaches and then study the crossover between the respective regimes.

*AH Model.*—We consider the AH Hamiltonian,  $H = H_m + H_t + H_l$ , describing a molecular level with tunnel coupling ( $H_t$ ) to metallic source and drain contacts. Taking a single spinless dot level (fermion annihilation operator  $d$ ) with energy  $\epsilon$  and a boson mode (annihilation operator  $b$ ) of frequency  $\Omega$ , the isolated molecule Hamiltonian is [3] (we use units with  $\hbar = k_B = 1$ )

$$H_m = \Omega b^\dagger b + [\epsilon + \lambda(b + b^\dagger)] n_d \quad (1)$$

with  $n_d = d^\dagger d$  and the electron-phonon coupling strength  $\lambda$ . The lead Hamiltonian  $H_l$  is taken in the standard wide-band approximation [23], with relaxation processes

assumed fast enough to have Fermi functions with temperature  $T$  as electronic distributions; their chemical potential difference defines the bias voltage  $V$ . The tunnel coupling then introduces the hybridization energy scales  $\Gamma_L$  and  $\Gamma_R$  for the left/right lead [23]. For simplicity, we focus on the symmetric case in what follows,  $\Gamma_L = \Gamma_R = \Gamma/2$ . As observable of main interest, we study the steady-state current  $I$  through the molecule.

*Analytical approaches.*—Before turning to a description of the ISPI scheme, let us briefly summarize the analytical approaches to the AH model that we employ to benchmark our method. (i) For  $\lambda/\Gamma \ll 1$ , perturbation theory in the electron-phonon coupling applies and yields a closed  $IV$  expression for arbitrary values of all other parameters [24]. We note that the solution of the AH model with a very broad dot level [25, 26] corresponds to this small- $\lambda$  regime. (ii) For high temperatures,  $T \gg \Gamma$ , a description in terms of a rate equation is possible [23]. We here use the simplest sequential tunneling version with golden rule rates [27]. For small  $\lambda$ , the corresponding results match those of perturbation theory, while in the opposite strong-coupling limit, the Franck-Condon blockade occurs and implies a drastic current suppression at low bias voltage [8, 28]. (iii) For small oscillator frequency,  $\Omega \ll \min(\Gamma, eV)$ , the nonequilibrium Born-Oppenheimer (NEBO) approximation is controlled and allows to obtain  $I$  from a Langevin equation for the oscillator [29, 30]. For small  $\lambda$ , this approach is also consistent with perturbative theory, while for high  $T$ , NEBO and rate equation results are found to agree.

*Keldysh path-summation formulation.*—We now start from the textbook time-discretized coherent-state representation of the Keldysh generating functional [31, 32]. The short-time propagator on the forward/backward branch of the Keldysh contour,  $e^{\mp i\delta_t H}$ , where  $\delta_t$  denotes the discrete time step, then allows for a Trotter breakup,  $e^{\mp i\delta_t H} = e^{\mp i\delta_t H_1} e^{\mp i\delta_t (H - H_1)}$ , with the systematic error in observables scaling  $\sim \delta_t^2$ . It is useful to choose  $H_1 = H_m - \Omega b^\dagger b$ , see Eq. (1), where the auxiliary relation

$$e^{\mp i\delta_t H_1} = 1 - n_d + n_d e^{-\lambda^2 \delta_t^2 / 2} e^{\mp i\delta_t \epsilon} e^{\mp i\delta_t \lambda b^\dagger} e^{\mp i\delta_t \lambda b} \quad (2)$$

allows to effectively decouple the electron-phonon interaction in terms of a three-state variable  $s_\eta = 0, \pm 1$  defined at each (discretized) time step  $t_j$  along the forward/backward ( $\sigma = \pm$ ) part of the Keldysh contour, where  $\eta = (t_j, \sigma)$ . Below, we also use the notation  $\eta \pm 1 = (t_{j \pm 1}, \sigma)$  with periodic boundary conditions on the Keldysh contour. It is crucial for the construction of the coherent-state functional integral that Eq. (2) is normal ordered. The “spin” variable  $s_\eta$  picks up the three terms in Eq. (2) and acts like a Hubbard-Stratonovich auxiliary field, similar to the Ising field employed in the Hirsch-Fye formulation of the Anderson model [19, 33]. The bosonic (phonon) scalar field and the fermionic (dot and lead electrons) Grassmann fields appearing in the

Keldysh path integral are then effectively noninteracting but couple to the time-dependent auxiliary spin variable. Hence those fields can be integrated out analytically and the time-dependent current,  $I(t_j)$ , follows from a path-summation formula for the generating functional,

$$\mathcal{Z} = \sum_{\{s_\eta=0,\pm 1\}} \det D[\{s\}], \quad (3)$$

where the matrix  $D_{\eta\eta'}$  (in time and Keldysh space) depends on the complete spin path  $\{s\}$ . Specifically, we obtain  $D = -iB(G_d^{-1} - \Sigma)$ , where  $G_d^{-1}$  is the discretized inverse Green’s function of the dot as in Refs. [19, 31] but with the modified spin-dependent matrix elements  $[-iG_d^{-1}]_{\eta+1,\eta} = -s_\eta$ . The self-energy matrix  $\Sigma$  describes the traced-out leads. We find  $\Sigma_{\eta\eta'} \neq 0$  only when  $s_\eta = \pm 1$ , where it coincides with the usual (wide-band limit) expression [23]. Finally, the diagonal matrix  $B$  (quoted here for  $\epsilon = 0$ ) with

$$B_{\eta\eta} = A_{s_\eta} e^{-\lambda^2 \delta_t^2 \sum_{\eta'} \sigma \sigma' [iG_{ph}]_{\eta,\eta'+1} |s_\eta s_{\eta'}|} \quad (4)$$

encapsulates all phonon effects, where  $G_{ph}$  is the discretized phonon Green’s function, see Ref. [31], and we used the notation  $A_0 = 1$  and  $A_{\pm 1} = \pm(1/2)e^{-\lambda^2 \delta_t^2 / 2}$ . By including a source term in  $D$ , it is straightforward to numerically extract the time-dependent current  $I(t_j)$  [19]. For sufficiently long times  $t_j$ ,  $I(t_j)$  reaches a plateau yielding the steady-state current of interest.

*ISPI implementation.*—Starting from the formally exact path-summation formula [Eq. (3)], the ISPI algorithm can now be adapted from Ref. [19]: For finite  $T$  or  $V$ , matrix entries  $D_{\eta\eta'}$  involving large time differences  $|t - t'|$  are exponentially small. We put these to zero beyond a memory time  $\tau_m \equiv K\delta_t$ , where  $K$  denotes the number of time slices kept in the memory. The numerical computation of the memory-truncated path summation in Eq. (3) is then possible in an iterative way [19] without additional approximations and, for given  $\delta_t$  and  $K$ , yields the steady-state current  $I(\delta_t, K)$ . While this formulation is exact for  $\delta_t \rightarrow 0$  and sufficiently large  $K$  (long memory time),  $K$  cannot be chosen arbitrarily large in practice and an extrapolation scheme is necessary [19]. Convergence of the extrapolation requires sufficiently high  $T$  or  $V$ , for otherwise the necessary memory times are exceedingly long. For the results below, we used  $K \leq 4$  and  $0.3 \leq \Gamma\delta_t \leq 0.35$ . The shown current follows by averaging over the  $\delta_t$ -window, with error bars indicating the mean variance. Additional ISPI runs for  $0.18 \leq \Gamma\delta_t \leq 0.22$  and  $0.3 \leq \Gamma\delta_t \leq 0.4$  were consistent with these results, and we conclude that small error bars indicate that convergence has been reached. For typical parameters and  $K = 4$ , our ISPI code yielding  $I(\delta_t, K)$  runs for  $\approx 11$  CPU hours on a 2.93 GHz Xeon processor.

*Benchmark checks.*—Next we show that the numerical ISPI results are consistent with analytical theory for the  $IV$  curves in all three parameter limits mentioned above.

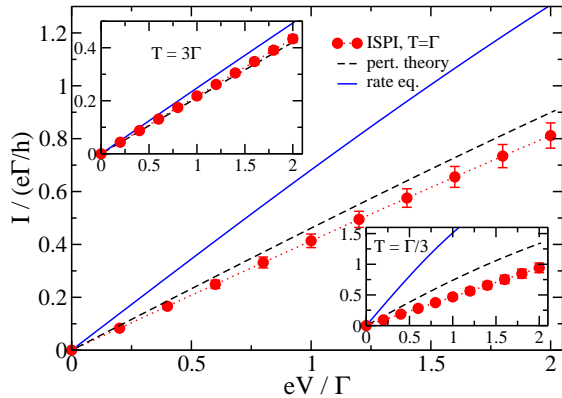


Figure 1. (Color online) Current  $I$  (in units of  $e\Gamma/h$ ) vs bias voltage  $V$  (in units of  $\Gamma/e$ ) for  $\lambda = 0.5\Gamma$ ,  $\Omega = \Gamma$ ,  $\epsilon = 0$ , and  $T = \Gamma$ . The ISPI data are depicted as filled red circles, where the dotted red curve is a guide to the eye only and the error bars are explained in the main text. We also show the results of perturbation theory in  $\lambda$  (dashed black curve) and of the rate equation (solid blue curve). The upper (lower) inset shows the corresponding result for  $T = 3\Gamma$  ( $T = \Gamma/3$ ).

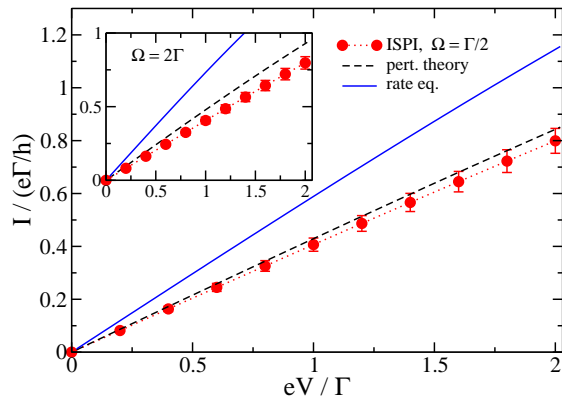


Figure 2. (Color online) Same as Fig. 1 but for  $\Omega = 0.5\Gamma$  (main panel) and  $\Omega = 2\Gamma$  (inset), both for  $T = \Gamma$ .

For clarity, we focus on a resonant level with  $\epsilon = 0$  here. Let us then start with the case of weak electron-phonon coupling,  $\lambda = 0.5\Gamma$ . Figure 1 compares our ISPI data for  $\Omega = \Gamma$  to the respective results of perturbation theory in  $\lambda$  and of the rate equation. As expected, for this parameter choice, perturbation theory essentially reproduces the ISPI data. The rate equation is quite accurate for high temperatures, but quantitative agreement with ISPI was obtained only for  $T \gtrsim 10\Gamma$ . Note that the ISPI error bars increase when lowering  $T$  due to the growing

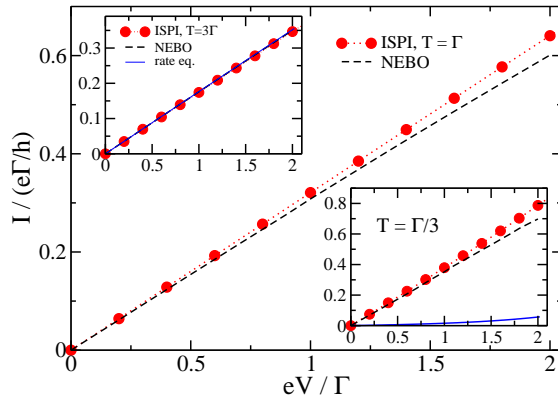


Figure 3. (Color online) Same as Fig. 1 but for  $\Omega = 0.5\Gamma$  and  $\lambda = \Gamma$ . The main panel is for  $T = \Gamma$  and compares the ISPI results to NEBO predictions. The insets are for  $T = 3\Gamma$  and  $T = \Gamma/3$ , respectively, where also the rate equation results are shown. Notice that in contrast to ISPI, the rate equation predicts an unphysical current blockade for  $T = \Gamma/3$ .

memory time ( $\tau_m$ ) demands. The effect of changing the phonon frequency  $\Omega$  is illustrated in Fig. 2, taking  $T = \Gamma$  but otherwise identical parameters. Again perturbation theory is well reproduced. Next, Fig. 3 shows ISPI results for a slow phonon mode,  $\Omega = \Gamma/2$ , with stronger electron-phonon coupling,  $\lambda = \Gamma$ . In that case, perturbation theory in  $\lambda$  is not reliable and the rate equation is only accurate at the highest temperature ( $T = 3\Gamma$ ) studied, cf. the upper left inset of Fig. 3. However, we observe from Fig. 3 that for such a slow phonon mode, NEBO provides a good approximation for all temperatures and/or voltages of interest. We conclude that the ISPI technique is capable of accurately describing three different analytically tractable parameter regimes.

*Franck-Condon (FC) blockade.*—Next we address the limit of strong electron-phonon coupling  $\lambda$ , where the rate equation approach yields a FC blockade of the current for low bias and  $T \gg \Gamma$  [28]. Sufficiently large  $\lambda$  can be realized experimentally, and the FC blockade has indeed been observed in suspended carbon nanotube quantum dots [8]. For an unequilibrated phonon mode with intermediate-to-large  $\lambda$ , understanding the FC blockade in the quantum-coherent low-temperature regime,  $T < \Gamma$ , is an open theoretical problem. Here multiple phonon excitation and deexcitation effects imply a complicated (unknown) nonequilibrium phonon distribution function, and the one-step tunneling interpretation in terms of FC matrix elements between shifted oscillator parabolas [28] is not applicable anymore. We here study this question using ISPI simulations, which automatically take into account quantum coherence effects.

In Fig. 4, the crossover from weak to strong electron-

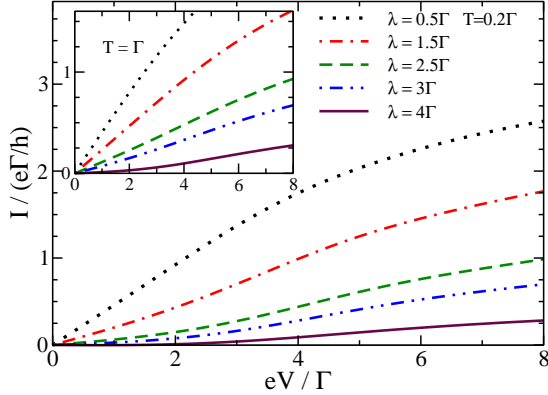


Figure 4. (Color online) ISPI data for the  $IV$  curves from weak ( $\lambda = 0.5\Gamma$ ) to strong ( $\lambda = 4\Gamma$ ) electron-phonon coupling, with  $\Omega = 2\Gamma$ . The main panel is for  $T = 0.2\Gamma$ , the inset for  $T = \Gamma$ . We used a dense voltage grid yielding smooth  $IV$  curves. Error bars are not shown but remain small, cp. Fig. 1.

phonon coupling  $\lambda$  is considered. The inset shows  $IV$  curves for  $T = \Gamma$ , where we observe a current blockade for low voltages once  $\lambda \gtrsim 2\Gamma$ . The blockade becomes more pronounced when increasing  $\lambda$  and is lifted for voltages above the polaron energy  $\lambda^2/\Omega$  [28]. Remarkably, the FC blockade persists and becomes even sharper as one enters the quantum-coherent regime (here,  $T = 0.2\Gamma$ ), despite of the breakdown of the sequential tunneling picture. We also observe a nonequilibrium smearing of phonon step features in the  $IV$  curves in Fig. 4, cf. also Refs. [8, 28].

**Conclusions.**—We have extended the iterative simulation of path integrals (ISPI) technique to the Anderson-Holstein model, which is the simplest nonequilibrium model for quantum dots or molecules with an intrinsic bosonic (phonon) mode. Our formulation exploits a mapping to an effective three-state system and reproduces three analytical theories valid in different parameter regions. This extension of the ISPI approach then captures the full crossover between those limits unless both  $T$  and  $V$  are very small. For strong electron-phonon coupling and an unequilibrated phonon mode, we find that the Franck-Condon blockade becomes even more pronounced as one enters the quantum coherent regime.

We thank A. Zazunov for helpful discussions. Financial support by the DFG (SPP 1243 and SFB 668) and by the ZIM (Düsseldorf) is acknowledged.

[1] J.C. Cuevas and E. Scheer, *Molecular electronics: An Introduction to Theory and Experiment* (World Scientific, Singapore, 2010).

- [2] N.A. Zimbovskaya and M.R. Pederson, *Phys. Rep.* **509**, 1 (2011).
- [3] M. Galperin, M.A. Ratner, and A. Nitzan, *J. Phys.: Cond. Matt.* **19**, 103201 (2007).
- [4] H.G. Craighead, *Science* **290**, 1532 (2000); M.L. Roukes, *Phys. World* **14**, 25 (2001).
- [5] O. Tal, M. Krieger, B. Leerink, and J.M. van Ruitenbeek, *Phys. Rev. Lett.* **100**, 196804 (2008).
- [6] G.A. Steele, A.K. Hüttel, B. Witkamp, M. Poot, H.B. Meerwaldt, L.P. Kouwenhoven, and H.S.J. van der Zant, *Science* **325**, 1103 (2009).
- [7] B. Lassagne, Y. Tarakanov, J. Kinaret, D. Garcia-Sanchez, and A. Bachtold, *Science* **325**, 1107 (2009).
- [8] R. Leturcq, C. Stampfer, K. Inderbitzin, L. Durrer, C. Hierold, E. Mariani, M.G. Schultz, F. von Oppen, and K. Ensslin, *Nature Phys.* **5**, 327 (2009).
- [9] A. K. Hüttel, B. Witkamp, M. Leijnse, M.R. Wegewijs, and H.S.J. van der Zant, *Phys. Rev. Lett.* **102**, 225501 (2009).
- [10] A. Mitra, I. Aleiner, and A.J. Millis, *Phys. Rev. B* **69**, 245302 (2004).
- [11] H. Wang and M. Thoss, *J. Chem. Phys.* **131**, 024114 (2009).
- [12] P.S. Cornaglia, H. Ness, and D.R. Grempel, *Phys. Rev. Lett.* **93**, 147201 (2004).
- [13] L. Arrachea and M.J. Rozenberg, *Phys. Rev. B* **72**, 041301(R) (2005).
- [14] E. Gull, A.J. Millis, A.I. Lichtenstein, A.N. Rubtsov, M. Troyer, and P. Werner, *Rev. Mod. Phys.* **83**, 349 (2011).
- [15] J.E. Han, *Phys. Rev. B* **81**, 113106 (2010).
- [16] A. Dirks, P. Werner, M. Jarrell, and T. Pruschke, *Phys. Rev. E* **82**, 026701 (2010).
- [17] L. Mühlbacher and E. Rabani, *Phys. Rev. Lett.* **100**, 176403 (2008).
- [18] M. Schiró and M. Fabrizio, *Phys. Rev. B* **79**, 153302 (2009).
- [19] S. Weiss, J. Eckel, M. Thorwart, and R. Egger, *Phys. Rev. B* **77**, 195316 (2008); *ibid.* **79**, 249901(E) (2009).
- [20] J. Eckel, F. Heidrich-Meisner, S.G. Jakobs, M. Thorwart, M. Pletyukhov, and R. Egger, *New J. Phys.* **12**, 043042 (2010).
- [21] D. Segal, A.J. Millis, and D.R. Reichman, *Phys. Rev. B* **82**, 205323 (2010).
- [22] For an equilibrated mode, i.e., in the presence of a secondary phonon bath, both ISPI and other numerical schemes [11, 17, 18] simplify substantially.
- [23] Yu.V. Nazarov and Ya.M. Blanter, *Quantum Transport* (Cambridge University Press, 2010).
- [24] R. Egger and A.O. Gogolin, *Phys. Rev. B* **77**, 113405 (2008).
- [25] B. Dorá and A. Halbritter, *Phys. Rev. B* **80**, 155402 (2009).
- [26] Y. Vinkler, A. Schiller, and N. Andrei, *Phys. Rev. B* **85**, 035411 (2012).
- [27] S. Braig and K. Flensberg, *Phys. Rev. B* **68**, 205324 (2003).
- [28] J. Koch and F. von Oppen, *Phys. Rev. Lett.* **94**, 206804 (2005).
- [29] F. Pistolesi, Ya.M. Blanter, and I. Martin, *Phys. Rev. B* **78**, 085127 (2008).
- [30] N. Bode, S. Viola Kusminskiy, R. Egger, and F. von Oppen, *Phys. Rev. Lett.* **107**, 036804 (2011).
- [31] A. Kamenev and A. Levchenko, *Adv. Phys.* **58**, 197 (2009).

- [32] A. Altland and B.D. Simons, *Condensed Matter Field Theory*, 2nd ed. (Cambridge University Press, 2010).
- [33] J.E. Hirsch and R.M. Fye, Phys. Rev. Lett. **56**, 2521 (1986).